Available online at www.sciencedirect.com
SCIENCE DIRECT®
Journal of Catalysis 223 (2004) 200–211
JOURNAL OF CATALYSIS
www.elsevier.com/locate/jcat

Investigations into the origin of the remarkable catalytic performance of aged H-ferrierite for the skeletal isomerization of 1-butene to isobutene

Song-Ho Lee,[a] Chae-Ho Shin,[a] and Suk Bong Hong [b,*]

[a] *Department of Chemical Engineering, Chungbuk National University, Chungbuk 361-763, South Korea*
[b] *Division of Chemical Engineering, Hanbat National University, Taejon 305-719, South Korea*

Received 20 October 2003; revised 19 January 2004; accepted 28 January 2004

Abstract

The catalytic properties of the proton form of six different 10-ring zeolites (clinoptilolite, ferrierite, ZSM-22, SUZ-4, ZSM-57, and ZSM-5), together with the dealuminated analogs of some of these materials prepared via oxalic acid treatment, are compared in the skeletal isomerization of 1-butene. While the pore shape of 10-ring channels in this series of medium-pore zeolites was found to be the key parameter substantially governing the isomerization activity, the catalytic data obtained from two H-ferrierites with similar Si/Al ratios but different crystal sizes reveal that the rate of coke formation on this particular zeolite structure, as well as its isobutene selectivity, can differ significantly according to the zeolite crystal size. The overall results of our study strongly suggest that the remarkable isobutene selectivity of aged H-ferrierite is a consequence of pore mouth shape catalysis over the Brønsted acid sites located near the 10-ring pore mouths with a suitable degree of ellipticity, which may come not only from the unique geometrical constraints imposed by the dual pore system of this particular zeolite, but also from its behavior of being normally synthesized with a submicrometer crystal size.

Keywords: 1-Butene skeletal isomerization; Aged H-ferrierite; High isobutene selectivity; Coke formation; Pore mouth catalysis

1. Introduction

Apart from the industrial point of view, the skeletal isomerization of *n*-butenes to isobutene has long been of academic interest as well, because of its difficulty in being catalyzed by conventional solid acids [1,2]. It was in the early 1990s when Shell scientists offered a major breakthrough in this field of research: the proton form of zeolite ferrierite (H-FER), which contains a two-dimensional pore system consisting of 10-ring (4.2 × 5.4 Å) channels intersected by 8-ring (3.5 × 4.8 Å) channels, is much more effective than any of the earlier catalysts for steering the isomerization of *n*-butenes toward the skeletal isomer rather than nonselective side reactions such as dimerization followed by cracking into light hydrocarbons [3,4]. An intriguing, recurring question regarding the isomerization activity of this medium-pore zeolite is the rapid increase in selectivity to isobutene with increasing time on stream (TOS) [4–6]. While the initial isobutene selectivity is rather poor, therefore, the high selectivity together with fairly good stability is normally observed only over the aged catalyst with carbonaceous deposits present, implying changes in the prevailing reaction mechanism. When ^{13}C-enriched 1-butene is reacted with H-FER [7,8], in fact, the extensive ^{13}C scrambling was found at the beginning of the reaction, indicating that the initial isobutene formation is dominated by nonselective bimolecular reactions, i.e., dimerization followed by cracking. Although with prolonged TOS hardly any scrambling was observed, in contrast, the precise mechanism by which isobutene is produced in the long run is still subject to vigorous debate [4,7,9–14]. In addition, the nature and location of catalytically active sites (mainly Brønsted acid sites) for *n*-butene skeletal isomerization over the aged catalyst, as well as the exact role of deposited coke, have been of much interest and controversy.

The purpose of the present study is to gain new insights into these issues. While H-FER is to date the most extensively studied and best catalyst for *n*-butene skeletal isomerization, the catalytic properties of many other zeolites and related microporous materials with different framework structures and compositions for this reaction have also been

* Corresponding author.
E-mail address: sbhong@hanbat.ac.kr (S.B. Hong).

0021-9517/$ – see front matter
doi:10.1016/j.jcat.2004.01.029

investigated [15–17]. Apparently, their pore size is the most important feature with regard to isobutene selectivity and stability, since all the molecular sieves reported as selective isomerization catalysts have 10-ring channels. However, not all the medium-pore materials are selective for this isomerization. For example, H-SUZ-4 with two perpendicular intersecting 10- and 8-ring channels [18], the pore architecture of which is thus the same as that of FER, but for which the 10-ring channels are slightly more circular in the former zeolite (4.6 × 5.2 Å vs 4.2 × 5.4 Å), was reported to exhibit a considerably lower activity than the latter zeolite [19]. This has led us to focus on the "pore shape" of medium-pore zeolites as a more crucial parameter governing their isomerization activities. Here we present the catalytic properties of the proton form of a series of 10-ring zeolites (i.e., clinoptilolite, FER, ZSM-22, SUZ-4, ZSM-57, and ZSM-5) with different degrees of ellipticity of their 10-ring pores for the skeletal isomerization of *n*-butenes, as well as those obtained from the dealuminated analogs of some of these zeolites, which were prepared via oxalic acid treatment [20,21], in order to elucidate the physicochemical properties of H-FER which allow this particular zeolite to have high isobutene selectivity from *n*-butenes. To clarify the location of Brønsted acid sites responsible for the selective formation of isobutene over H-FER, we have compared the isomerization activities of two H-FER and two H-ZSM-5 zeolites characterized by similar Al contents but different crystal sizes, respectively. Catalytic studies involving zeolite crystals with the precisely controlled compositions and crystal sizes are of extreme importance in elucidating the type of the shape-selective phenomena derived from the particular pore architecture of this class of microporous materials.

2. Experimental

Clinoptilolite (Si/Al = 5.8), FER (Si/Al = 9.0), ZSM-22 (Si/Al = 33), SUZ-4 (Si/Al = 8.2), and ZSM-57 (Si/Al = 25) were synthesized according to the procedures described in the literature [22–26]. For brevity's sake, we will refer to clinoptilolite simply as CLI in our study. Two NH_4-ZSM-5 zeolites with Si/Al = 13.5 and 27 were obtained from ALSI-PENTA Zeolithe. For comparison, in addition, large FER and ZSM-5 crystals having Si/Al ratios of 14.4 and 27, respectively, were prepared by the procedures given elsewhere [27,28]. All the materials prepared using organic structure-directing agents (SDAs) were calcined in air at 550 °C for 12 h to remove the organic species occluded. The calcined samples were then converted into their proton form by refluxing twice in 1.0 M NH_4NO_3 solutions (1.0 g solid per 100 mL solution) for 6 h followed by calcination at 550 °C for 8 h. Dealumination was carried out by refluxing 1.0 g of the proton form of zeolite samples in 100 mL of 1.0 M oxalic acid solutions for 1 or 24 h. After acid treatment zeolite particles were filtered off and washed first with cold and then hot distilled water, until all traces of remaining acid were removed. Finally, the dealuminated samples were dried in air room temperature and calcined at 500 °C for 4 h, prior to their use as catalysts.

Powder X-ray diffraction (XRD) patterns were collected on a Rigaku 2500H diffractometer with Cu-K_α radiation. All the materials prepared here were highly crystalline and no reflections other than those from each zeolite are observed. Chemical analysis was carried out by the Analytical Laboratory of Korea Institute of Science and Technology. The Si/Al ratios in the superficial region of zeolite crystals were determined by X-ray photoelectron spectroscopy (XPS) with a VG ESCALAB 210 spectrometer employing an Mg-K_α X-ray source (1253.6 eV). Typically, 20 scans were accumulated and all the binding energies are referenced to the C($1s$) line at 284.6 eV from adventitious carbon. Then, the superficial Si/Al ratios were calculated from the Si($2p$) and Al($2p$) line intensities using appropriate sensitivity factors. Crystal morphology and size were determined by a JEOL JSM-6300 scanning electron microscope (SEM). Thermogravimetric analyses (TGA) were performed in air on a TA Instruments SDT 2960 thermal analyzer, where the weight loss related to the combustion of coke deposits formed during the 1-butene skeletal isomerization was further confirmed by differential thermal analyses (DTA) using the same analyzer. The N_2 sorption experiments were performed on a Micromeritics ASAP 2010 analyzer.

A conventional continuous-flow microreactor was used to carry out the skeletal isomerization of 1-butene over various medium-pore zeolites at atmospheric pressure. Prior to the experiments, the zeolite was routinely activated under flowing He (50 $cm^3\,min^{-1}$) at 500 °C for 1 h and kept at 400 °C to establish a standard operating procedure, allowing time for the product distribution to stabilize. Then, a reactant stream with a He/1-butene molar ratio of 9 to 1 was fed into a quartz reactor containing 0.1 g of zeolite catalyst at the same temperature. The total gas flow at the reactor inlet was kept constant at 50 $cm^3\,min^{-1}$. The reaction products were analyzed on-line in a Chrompack CP 9001 gas chromatograph equipped with an Al_2O_3/KCl Plot capillary column (0.53 mm × 50 m) and a flame ionization detector (FID), with the first analysis carried out after 5 min on stream. Conversion and selectivity to each product were calculated following the methods described elsewhere [9,26].

3. Results and discussion

The physical properties of all zeolites employed in this study, together with their formal designation, are listed in Table 1. These data reveal that oxalic acid treatment does not lead to a noticeable increase in bulk Si/Al ratios of dealuminated materials. However, the opposite is observed for their Si/Al ratios in the superficial region, which were determined by XPS to a depth of ∼ 50 Å. Powder XRD experiments show that the positions and relative intensities of all the X-ray peaks from dealuminated materials are essen-

Table 1
Characterization data for all the zeolite catalysts employed in this study

Catalyst ID[a]	IZA code	Si/Al ratio		Crystal shape and average size (μm)	BET surface area[d] ($m^2\ g^{-1}$)	Micropore volume[e] ($cm^3\ g^{-1}$)	Mesopore volume[f] ($cm^3\ g^{-1}$)	Amount (wt%) of coke deposited[g]
		Bulk[b]	Surface[c]					
H-CLI		5.8	6.1		254	0.101 (231)	0.041 (23)	6.3
H-CLI-D1	HEU	5.8	8.8	Rhombic platelets, 3.0×0.6	124	0.045 (113)	0.017 (11)	2.7
H-CLI-D24		6.4	16.9		131	0.053 (116)	0.026 (15)	2.9
H-FER		9.0	8.5		385	0.146 (359)	0.041 (26)	8.9
H-FER-D1	FER	9.4	14.3	Square platelets, $0.7 \times 0.7 \times 0.1$	384	0.144 (361)	0.036 (23)	7.7
H-FER-D24		9.5	16.5		393	0.149 (365)	0.049 (28)	7.9
H-FER-L		14.4	17.2	Square platelets, $20 \times 20 \times 1$	387	0.145 (381)	0.013 (6)	5.6
H-ZSM-22		33.4	34.9		215	0.082 (186)	0.068 (29)	1.9
H-ZSM-22-D1	TON	35.9	47.0	Needles, 0.6×0.1	208	0.080 (179)	0.068 (29)	1.6
H-ZSM-22-D24		39.1	55.0		176	0.067 (148)	0.064 (28)	1.5
H-SUZ-4	–	8.2	–[h]	Needles, 1.0×0.2	320	0.123 (290)	0.050 (30)	6.0
H-ZSM-57	MFS	24.7	–[h]	Square platelets, $0.6 \times 0.6 \times 0.1$	343	0.132 (260)	0.193 (83)	11.2
H-ZSM-5		13.5	13.7		389	0.150 (374)	0.022 (15)	9.3
H-ZSM-5-D1		13.5	14.6	Spherulites, 1–3	396	0.151 (379)	0.024 (17)	8.6
H-ZSM-5-D24	MFI	13.9	24.6		400	0.154 (380)	0.026 (20)	8.5
H-ZSM-5-S		27.0	28.5	Small spherulites, 0.1	333	0.130 (303)	0.048 (30)	5.8
H-ZSM-5-L		27.0	36.1	Coffins, $30 \times 10 \times 10$	405	0.165 (399)	0.015 (6)	6.1

[a] D1 and D24 indicate that the zeolites were dealuminated by being refluxed in 1.0 M oxalic acid solutions for 1 and 24 h, respectively. S and L denote that the crystal sizes of zeolites are small and large, respectively.

[b] Determined by chemical analysis.

[c] Determined by XPS elemental analysis.

[d] Calculated from N_2 adsorption data.

[e] Calculated from the volume of the adsorbed N_2 at $P/P_0 = 0.1$, corresponding to the pore diameter of ca. 20 Å. The values given in parentheses are micropore areas in $m^2\ g^{-1}$ calculated using the *t*-plot method.

[f] In the diameter range 20–500 Å. The values given in parentheses are external surface areas in $m^2\ g^{-1}$ calculated using the *t*-plot method.

[g] Determined from TGA/DTA after the skeletal isomerization of 1-butene at 400 °C for 8 h. The other reaction conditions are the same as those stated in the text.

[h] Not determined.

tially the same as those from the corresponding, parent materials. Also, no noticeable changes in their crystal size and morphology are detected from SEM measurements. As previously reported by Apelian et al. [20], therefore, it is clear that oxalic acid treatment removes the surface/near-surface Al atoms of medium-pore zeolites more selectively than Al in the interior without changing crystal morphology and integrity, which is important for elucidating the role of acid sites on/near the external surface for the skeletal isomerization of *n*-butenes to isobutene over various 10-ring zeolites studied here. Table 1 also gives the N_2 adsorption data for the zeolites before and after oxalic acid treatment. When the dealuminated analogs of H-FER, H-ZSM-22, and H-ZSM-5 are compared to the corresponding, parent materials, no significant changes in the micropore volume are observed, revealing that their structural integrity remains intact during the dealumination process, as evidenced by powder XRD measurements. However, H-CLI exhibits a notable decrease in micropore volume, as well as in mesopore volume (or in external surface area), after oxalic acid treatment. XPS elemental analysis indicates that this zeolite has the highest Al content in the superficial region among the zeolites used in this study (Table 1). Then, it can be expected that the amount of framework Al atoms removed not only from the outer surface of zeolite crystals during the oxalic acid treatment, but also from their near surface (e.g., 10-ring pore mouth inlets), should be much larger on H-CLI than on the other zeolites with lower Al contents, leading to a more serious collapse of the surface/near-surface structure. Furthermore, the 10-ring channels in CLI are much more elliptical than those in any of the other 10-ring materials employed here. Therefore, it is most likely that a considerable fraction of the 10-ring pore mouth inlets in H-CLI becomes inaccessible for N_2 molecules upon treating with oxalic acid, which must be responsible for the observed decrease in micropore volume. However, the dealuminated CLI analogs appear to maintain their overall structure, since all the characteristic X-ray peaks of CLI remained intact even after the acid treatment step.

Fig. 1 shows 1-butene conversion and isobutene selectivity and yield as a function of TOS in the skeletal isomerization of 1-butene over H-CLI, H-FER, H-ZSM-22, H-SUZ-4, H-ZSM-57, and H-ZSM-5 measured at 400 °C and 10.1 kPa 1-butene in the feed. The major by-product (i.e., propene and pentenes) selectivities and yields are also given in Fig. 1. While the acidic properties of zeolites are crucial for the rate of coke formation which has a great influence on the activity, selectivity, and stability of this class of microporous materials during the isomerization reaction, it has been repeatedly shown that their pore structure is the most important feature with regard at least to the initial isobutene selectivity [7–17,29]. To minimize the secondary effect of

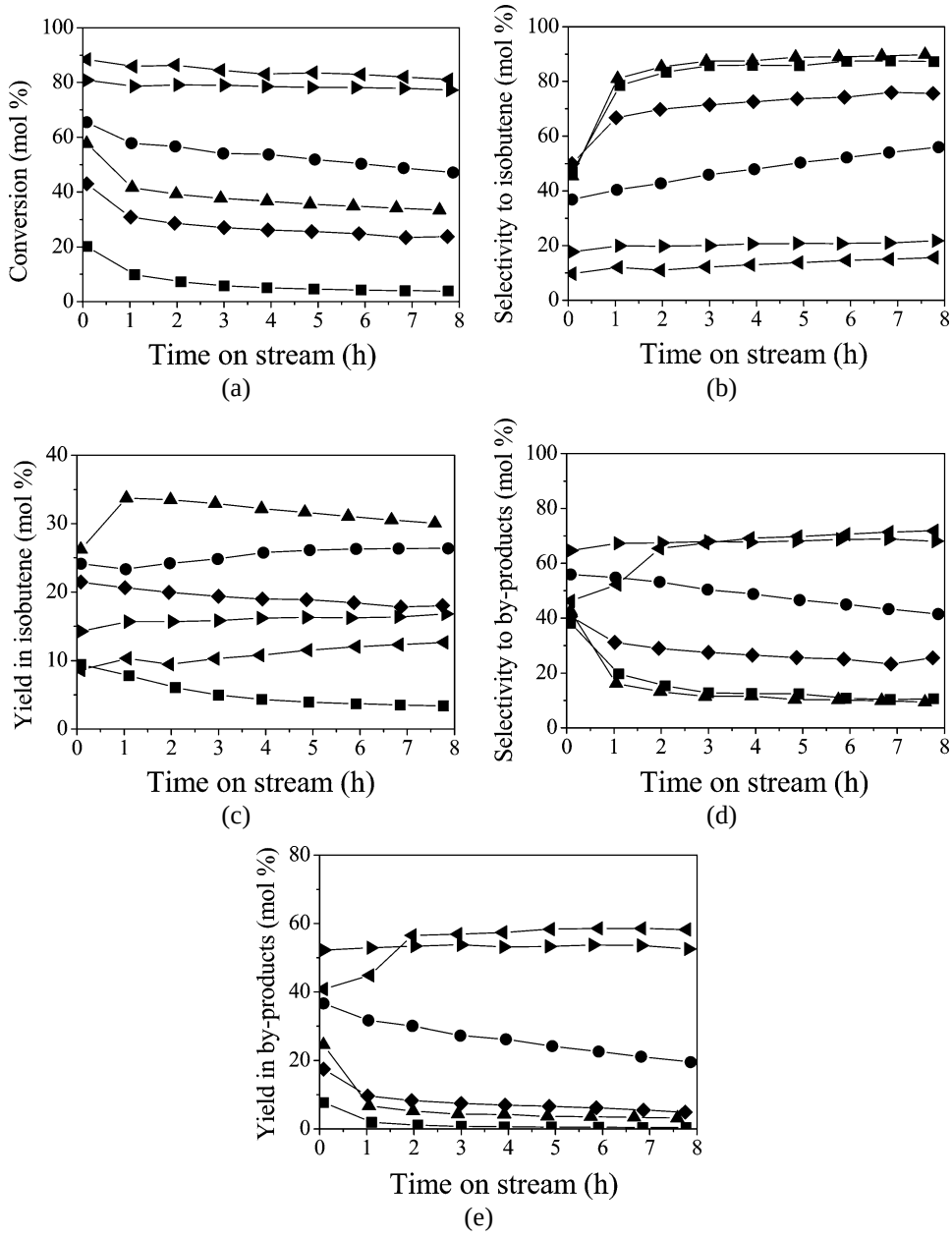

Fig. 1. (a) 1-Butene conversion, (b) selectivity to isobutene, (c) yield in isobutene, (d) selectivity to major by-products (i.e., propene plus pentenes), and (e) yield in major by-products as a function of time on stream in skeletal isomerization of 1-butene over H-CLI (■), H-FER (▲), H-ZSM-22 (●), H-SUZ-4 (◆), H-ZSM-57 (►), and H-ZSM-5 (◄) at 400 °C and 10.1 kPa 1-butene pressure.

coke deposition on the selectivity to isobutene, therefore, we have regarded the results obtained at 5 min on stream as the intrinsic activities of 10-ring zeolite catalysts used here [26,30,31]. When the six 10-ring zeolites are compared with one another under the same reaction conditions, the initial 1-butene conversion was found to be higher in the order H-CLI < H-SUZ-4 < H-FER < H-ZSM-22 < H-ZSM-57 < H-ZSM-5. As seen in Fig. 1, in contrast, the initial isobutene selectivity increases in the order H-ZSM-5 < H-ZSM-57 < H-ZSM-22 < H-FER ≈ H-CLI ≈ H-SUZ-4. Among the six 10-ring zeolites, consequently, H-FER and H-ZSM-22 show high initial isobutene yield while the opposite is observed for the other four materials. The crystallographic pore dimensions of 10-ring channels in these six zeolites, together with their ellipticity (ε) values, are given in Table 2. Here, we have taken the ellipticity which is defined by $\{(b^2 - a^2)/b^2\}^{0.5}$ [32], where a and b are the shortest and longest pore diameters, respectively, as a quantitative measure of differences in the 10-ring pore shape. Plots of the isomerization activities of all the six zeolites with different structures measured after 5 min and 8 h on stream corresponding to the ellipticity of their 10-ring channels are shown in Fig. 2. In the case of ZSM-5 with an intersecting 10-ring pore system between the straight and the sinusoidal channels, the catalytic data are plotted with the average value (0.349) of the ellipticities of its two 10-ring pores. Fig. 2 reveals that in

Table 2
Pore dimensions and ellipticities of 10-ring channels in zeolites studied here

Zeolite	Pore topology	10-Ring pore size (Å) and area[a] (Å^2)	ε[b]
CLI	2D, 10- and 8-rings	3.1 × 7.5, 18.3	0.911
FER	2D, 10- and 8-rings	4.2 × 5.4, 17.8	0.629
ZSM-22	1D, 10-rings	4.6 × 5.7, 20.6	0.591
SUZ-4	2D, 10- and 8-rings	4.6 × 5.2, 18.8	0.466
ZSM-57	2D, 10- and 8-rings	5.1 × 5.4, 21.6	0.329
		5.1 × 5.5, 22.0 (sinusoidal)	0.374
ZSM-5	3D, 10-rings	5.3 × 5.6, 23.3 (straight)	0.323

[a] Calculated using the equation $A = \pi ab/4$, where A, a, and b are the pore area and the shortest and longest 10-ring pore diameters, respectively. The 10-ring pores in each zeolite are assumed to be ideally elliptical in shape.

[b] Ellipticity defined as $\{(b^2 - a^2)/b^2\}^{0.5}$.

general, the more elliptical 10-ring channels the zeolite has, the lower 1-butene conversion but the higher initial isobutene selectivity it shows. It is interesting to note here that such a trend is also observed from the plots of the catalytic activities measured after 8 h on stream vs the ellipticity of 10-ring channels of each zeolite.

However, there is one exception (H-SUZ-4) to the order of classification with regard to the ellipticity of 10-ring pores, because the initial 1-butene conversion and selectivity to isobutene over H-SUZ-4 are considerably lower and higher than those observed for H-ZSM-22 with more elliptical 10-ring pores, respectively. According to the proposed framework topology by Lawton et al. [18], SUZ-4 has small cages between double 6-rings, serving as the site for nonexchangeable K^+ ions. In fact, chemical analysis has indicated that our H-SUZ-4 still contains a considerable amount (2.7 wt%) of K^+ ions even after $NH_4{}^+$ ion exchange. We believe that this may be the main reason for the catalytic behavior of H-SUZ-4, despite the relatively low degree of ellipticity of its 10-ring pores. In contrast, no general relationship between the isomerization activity of each zeolite and its 10-ring pore area or dimensionality was found, even if the 10-ring pore areas (20.8 ± 2.5 Å^2) of all the zeolites studied here are not significantly different from one another. Therefore, it is clear from Fig. 2 that the pore shape of 10-ring channels in medium-pore zeolites is the key parameter substantially governing the isomerization activity. However, the lack of a linear correlation between the initial 1-butene conversions or isobutene selectivities of all the six zeolites and the ellipticities of their 10-ring channels suggests that the effects of other factors including the zeolite crystal size and morphology on the isomerization activities of 10-ring zeolites could also be of considerable importance. On the other hand, it is not surprising to predict that the rate of diffusion of *n*-butene molecules into the intracrystalline space of a series of zeolites under study must be highly dependent on the degree of ellipticity of 10-ring pores, due to the similarity in their pore areas (Table 2). If such is the case, the

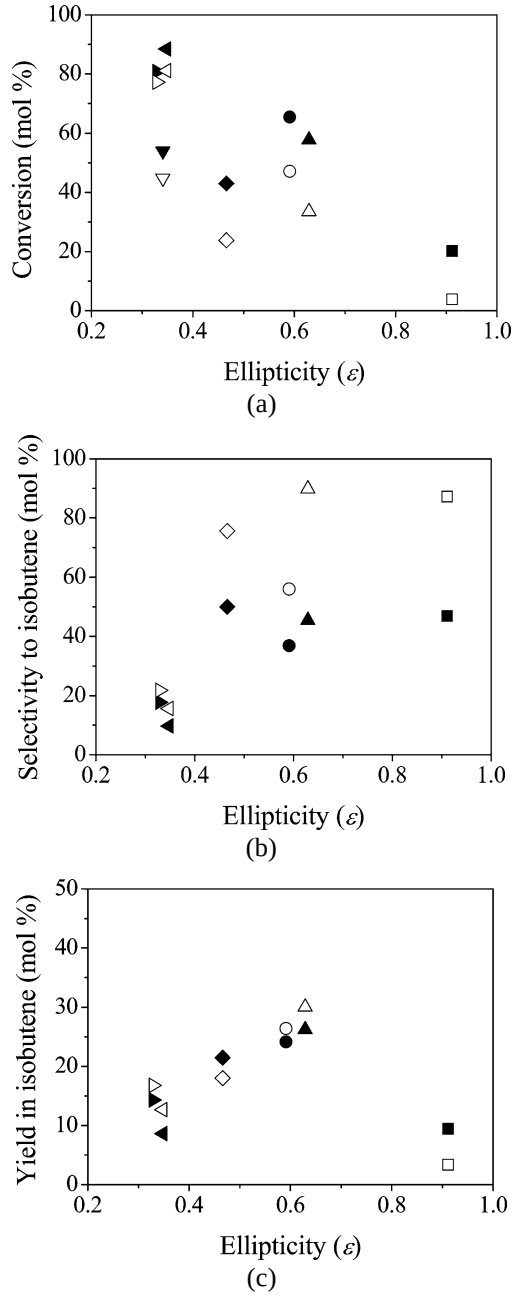

Fig. 2. Plots of (a) 1-butene conversion, (b) selectivity to isobutene, and (c) yield in isobutene in skeletal isomerization of 1-butene over H-CLI (■, □), H-FER (▲, △), H-ZSM-22 (●, ○), H-SUZ-4 (◆, ◇), H-ZSM-57 (►, ▷), and H-ZSM-5 (◄, ◁) analyzed after 5 min and 8 h on stream vs ellipticity of 10-ring channels of each zeolite. The reaction conditions are the same as those given in Fig. 1, and the catalytic data obtained after 5 min and 8 h on stream are indicated by closed and open symbols, respectively.

enhancement of initial isobutene selectivity with increasing the degree of ellipticity of 10-ring channels could be explained by the increasing pore constraints which gradually restrict the free diffusion of *n*-butenes and thus nonselective dimerization-cracking reactions due to the lower concentration of reactant molecules inside the zeolite pores. Also, an increase in initial 1-butene conversion with a decreasing degree of ellipticity of 10-ring channels in zeolites could be

understood in a similar manner. As seen in Fig. 1, however, high initial isobutene yield is observed only for H-FER and H-ZSM-22 but not for H-CLI or the other three zeolites with less elliptical 10-ring pores. This strongly suggests that to be an efficient isomerization catalyst, the 10-ring pores in medium-pore zeolite should not be too elliptical or circular. Another important result obtained from Fig. 1 is that a trend of rapidly increasing selectivity to isobutene at early TOS is much more apparent to H-CLI and H-FER with the two most elliptical 10-ring channels than to the other four zeolites. This implies that the prevailing mechanism for isobutene formation on the former two zeolites becomes altered over the period of TOS studied here, whereas such a change is less likely to occur over the latter four zeolites. Up to now, three major types of reaction pathways have been proposed for the acid-catalyzed isomerization of *n*-butenes to isobutene: monomolecular, pseudo-monomolecular, and bimolecular mechanisms [4–17]. While much discussion has been going on concerning the prevailing mechanism in the selective formation of isobutene over aged H-FER, there appears to be a general consensus that the nonselective dimerization mechanism is prevailing at least with fresh H-FER [7,8]. Fig. 1 shows that the catalytic selectivity of H-CLI is essentially the same as that observed for H-FER. This suggests that the prevailing mechanism over H-CLI at early TOS is also bimolecular.

Fig. 3 shows 1-butene conversion and selectivities to isobutene and to major by-products as a function of TOS in the skeletal isomerization over H-CLI, H-FER, H-ZSM-22, and H-ZSM-5 before and after oxalic acid treatment. In this set of comparative experiments the first two zeolites were selected because they show a rapid increase in selectivity to isobutene at early TOS (Fig. 1). Also, H-ZSM-22 and H-ZSM-5 were chosen due to their relative consistency in isobutene selectivity with TOS [26,33]. While there are two catalytic studies on dealuminated H-FER zeolites that were prepared in a manner similar to that employed here [34,35], no comparison with other 10-ring zeolites dealuminated by treating with oxalic acid has been made. Fig. 3 clearly shows that dealumination by treating with this carboxylic acid gives rise to notable changes in the isomerization activity of H-CLI and H-FER, whereas the opposite is observed for H-ZSM-22 and H-ZSM-5. Unlike their parent H-CLI zeolite, for example, both dealuminated CLI materials (i.e., H-CLI-D1 and H-CLI-D24) exhibit almost no 1-butene conversion from the beginning of the reaction. Although all three zeolite catalysts show similar initial isobutene selectivities, in addition, no significant increase in selectivity to isobutene with increasing TOS is observed from dealuminated analogs. One obvious reason for these results may be that oxalic acid treatment leads not only to the selective removal of surface/near-surface Al atoms of H-CLI, but also to the serious blockage of 10-ring pore mouth inlets, as already confirmed by a combination of XPS and N_2 sorption experiments. Further evidence to support this speculation can be obtained by comparing the levels (2.7–2.9%) of coke deposited on the dealuminated analogs of H-CLI during the 1-butene skeletal isomerization at 400 °C for 8 h, which were determined by TGA/DTA, with the amount (6.3%) of coke on used H-CLI (Table 1). Thus, the exact role of the Brønsted acid sites located at the 10-ring pore mouth inlets of CLI in this isomerization still remains unelucidated at this time. However, the fact that after some TOS the isobutene selectivities of both of the dealuminated CLI materials are much lower than the selectivity observed for the parent H-CLI zeolite, despite the presence of a nonnegligible amount of Al atoms in their surface/near surface, suggests that the acid sites present on the outer surface of zeolite crystals are not selective for formation of isobutene.

The most important observation obtained from Fig. 3 is that the two dealuminated H-FER catalysts give considerably lower 1-butene conversions than their parent zeolite, while there are no noticeable differences in the selectivity to isobutene or to by-products. Such a trend exits at least over the period of TOS studied here, and the extent of decrease in 1-butene conversion with TOS was found to be higher on the material treated with oxalic acid for a longer period of time. Apparently, this cannot be explained without considering that the density of the Brønsted acid sites near the 10-ring pore mouths of dealuminated FER zeolites is considerably low compared to the parent H-FER zeolite. Therefore, it is clear that not only those acid sites in H-FER play a role in selectively producing isobutene from the beginning of the reaction, but also after some TOS their contribution to the overall catalytic action of this zeolite increases rapidly as a consequence of extensive coke deposition inside the zeolite pores, certainly limiting the dimerization-cracking reactions. This means that a nonnegligible amount of isobutene formed over fresh H-FER is produced by the monomolecular mechanism, although the nonselective bimolecular mechanism is prevailing at early TOS. As already suggested by many different groups [7,9,10,15,36], in addition, it appears that the catalytic action of aged H-FER is dominated by the monomolecular mechanism, in which 1-butene is selectively isomerized over the Brønsted acid sites near the 10-ring pore mouths. In other words, pore mouth catalysis, which was initially proposed to explain the highly selective nature of medium-pore molecular sieves with a one-dimensional 10-ring pore system, such as ZSM-22 and SAPO-11, for the hydroisomerization of long-chain *n*-alkanes to their branched isomers [37–39], could be the main origin of the remarkable isobutene selectivity observed for aged H-FER. Three lines of reasoning to support this idea are given below. First, a recent series of studies by van Donk et al. [17,36,40,41] has shown that the 10-ring pore mouth inlets of aged H-FER are still accessible for 1-butene molecules, even in the case of deposition of high amounts (e.g., 6.8 wt%) of coke in the zeolite pores. Second, pore mouth shape selectivity allows us to explain the data of O'Young et al. [42] wherein H-FER is more selective than ZSM-23, despite the fact that the free diameter (5.2 Å) at the FER channel intersection is slightly larger than that (4.8 Å) of 10-ring channels in ZSM-

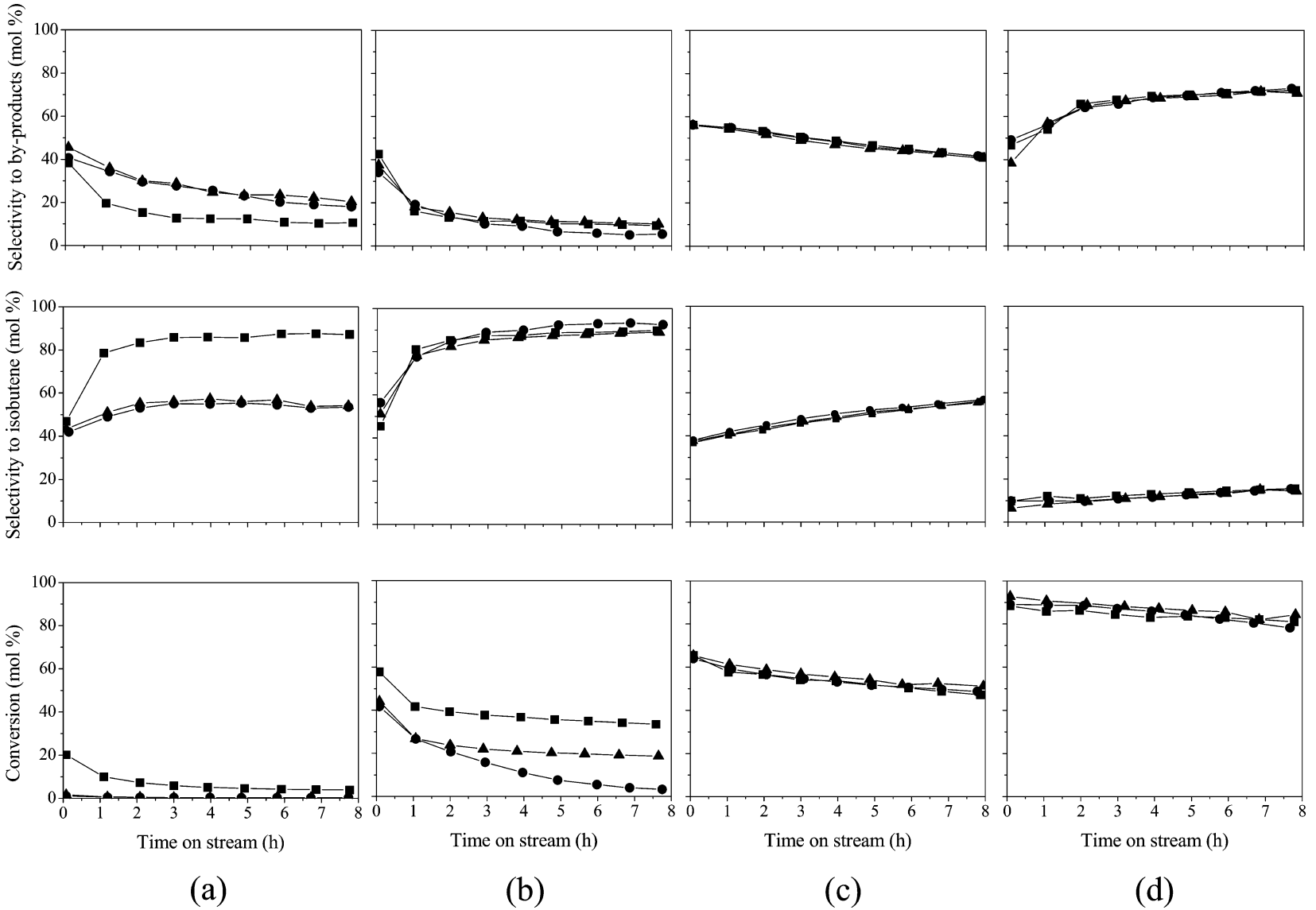

Fig. 3. 1-Butene conversion (bottom) and selectivities to isobutene (middle) and propene plus pentenes (top) as a function of time on stream in skeletal isomerization of 1-butene over (a) H-CLI, (b) H-FER, (c) H-ZSM-22, and (d) H-ZSM-5 before and after oxalic acid treatment. Squares indicate the materials before oxalic acid treatment, and triangles and circles indicate the two dealuminated analogs prepared by treating with oxalic acid for 1 and 24 h, respectively. The reaction conditions are the same as those given in Fig. 1.

23. Third, we found that the isomerization activities of two H-FER zeolites with similar Si/Al ratios but notably different crystal sizes and thus different numbers of 10-ring pore mouths per unit weight are significantly different from each other (see below).

The catalytic data in Fig. 3 also show that no detectable differences in the 1-butene conversion, as well as in the selectivity to isobutene or to by-products, over the period of TOS studied, are observed, when the dealuminated analogs of H-ZSM-22 are compared with the corresponding, parent zeolite under the same reaction conditions. The same trend can be observed from H-ZSM-5 and its dealuminated analogs. Therefore, it appears that unlike the case of aged H-FER, the acid sites located inside the 10-ring pores rather than near the 10-ring pore mouths still dictate the catalytic action of aged H-ZSM-22 and H-ZSM-5, on which the prevailing mechanism for isobutene formation may be preferentially bimolecular. This again reflects the importance of pore shape as a structural parameter influencing the isomerization reactivities of 10-ring zeolites, although the 10-ring channels in H-ZSM-22 are slightly more circular than those in H-FER. The monomolecular mechanism that undergoes a direct transformation of 1-butene to its skeletal isomer without the help of other 1-butene molecules, on the other hand, involves the formation of an energetically unfavorable primary carbenium ion [43]. As an alternative reaction pathway over used H-FER, therefore, Guisnet and co-workers have proposed the so-called pseudo-monomolecular mechanism in which the energetically more favorable alkylaromatic tertiary carbenium ions anchored to the coke deposited near the pore mouths may catalyze the selective production of isobutene [11–13]. The TGA/DTA results in Table 1 reveal that differences in the amount (8–9%) of coke formed on H-FER and its two dealuminated analogs during 8 h on stream are negligible. This suggests that the degrees of pore blockage of these three used materials by coke deposits may not be much different from one another. A quite similar result can also be observed from comparison of the dealuminated analogs of H-ZSM-22 and H-ZSM-5 with their parent, corresponding materials, respectively (Table 1). Clearly, if the pseudo-monomolecular mechanism exists, it could be very selective. However, one cannot claim that the creation of such highly selective sites, i.e., alkylaromatic tertiary carbenium ions, on the coke molecules located near the zeolite pore mouths is limited only to H-FER among the numerous 10-ring zeolites, even if coke formation on zeolites is a shape-selective process that is strongly influenced by the pore architecture of this class of microporous solids [44,45]. Because the pseudo-monomolecular mechanism does not require a large number of alkylaromatic tertiary carbenium ions to maintain high isobutene selectivity [13], the observed decrease in 1-butene conversion over H-FER caused by oxalic acid treatment makes the arguments against the existence of this mechanism stronger. In fact, there are several studies showing that the presence of coke deposits inside the H-FER pores is not crucial for achieving high isobutene selectivity [29,40,46,47], although they could contribute partly to the formation of by-products at early TOS.

Fig. 4 shows the SEM pictures of two pairs of H-FER and H-ZSM-5 crystals with similar bulk Si/Al ratios but dif-

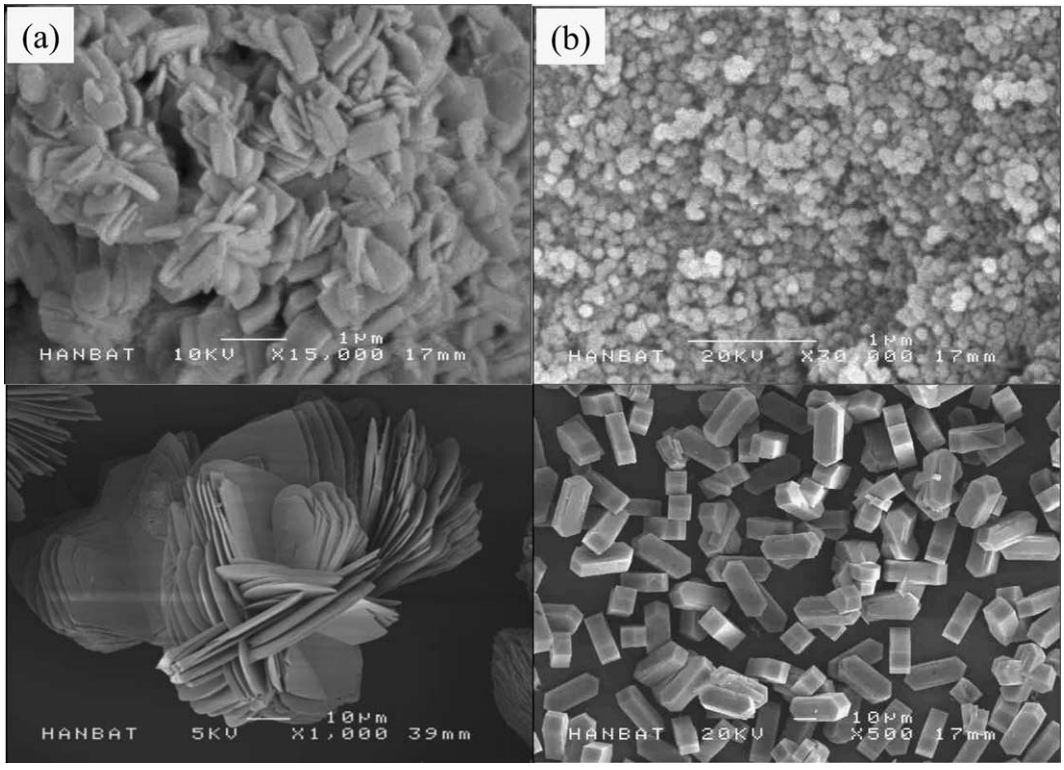

Fig. 4. SEM pictures of (a) H-FER and (b) H-ZSM-5 zeolites with small (top) and large (bottom) crystal sizes.

ferent crystal sizes, respectively. The small H-FER crystals, synthesized using pyrrolidine together with Na^+ [23], are characterized by a platelet-like shape of ca. 0.7 μm in base and 0.1 μm in thickness. For convenience's sake, we will denote this zeolite as H-FER-S from now on. A quite similar morphology is also observed from the large FER (i.e., H-FER-L) crystals with ca. 20 μm in base and 1 μm in thickness, which were prepared using 1,4-diaminobutane as an organic SDA in the absence of inorganic cations [27]. According to the high-resolution transmission electron microscopy (HRTEM) study by de Jong et al. [8], the 8- and 10-ring channels of the FER topology are perpendicular to the (010) and (001) surfaces of the platelet-like FER crystals, respectively, and are thus parallel to their basal plane. Assuming a square plate geometry for the two H-FER zeolites with different crystal sizes, the number of the 10-ring channels located at the boundary of H-FER-L crystals and thus available for pore mouth catalysis was calculated to be only 0.35% of that of the analogous channels at the boundary of the equivalent weight of H-FER-S crystals. While the same is also true for the ratio of the (001) surface areas of these two FER zeolites, the external surface area of H-FER-L derived from the *t*-plot method was found to be 23% of that for H-FER-S (Table 1), which is almost two orders of magnitude larger than the value calculated from the SEM data in Fig. 4. This discrepancy appears to originate from the heavily overlapped nature of FER crystals prepared here, as well as from the assumption of flat geometry and the limited accuracy of the method used in analyzing the N_2 sorption isotherms. However, we believe that even the difference determined from N_2 sorption data is still large enough to establish whether pore mouth shape catalysis occurs over aged H-FER. While H-ZSM-5-S consists of very small spherulites of ca. 0.1 μm, H-ZSM-5-L appears as well-faceted, coffin-shape crystals that are approximately 30 μm in length and 10 μm in height. Despite notable differences in the crystal morphology, as a result, a considerably smaller external surface area was also observed from H-ZSM-5-L. It should be noted here that these two pairs of zeolites with small and large crystal sizes exhibit no significant differences in their bulk and XPS elemental Si/Al ratios, respectively (Table 1). Thus, if we assume the statistical Al distribution throughout the FER or ZSM-5 crystals, the number of surface/near-surface acid sites generated by the presence of Al atoms in their frameworks should be considerably smaller for larger crystals, due to the much smaller external surface area. This implies that comparison of the 1-butene isomerization activities of a particular structure type of zeolites with similar Al contents but notably different crystal sizes could provide some insight into the location of acid sites dominating the catalytic events, no matter what selectivity to isobutene the zeolite employed shows.

Fig. 5 shows 1-butene conversion and selectivities to isobutene and major by-products as a function of TOS in the skeletal isomerization of 1-butene over H-FER-L and H-ZSM-5-L measured under the reaction conditions described above. Included for comparison are the isomerization activities of small H-FER-S and H-ZSM-5-S whose bulk Si/Al ratios are similar to those of H-FER-L and H-ZSM-5-L, respectively. It can be seen that H-FER-L gives a considerably higher 1-butene conversion than H-FER-S during the period of 8 h on stream, despite the similarity in their bulk and superficial Si/Al ratios. Of particular interest is the observation that the isobutene selectivity of the former zeolite is much lower from the beginning of the reaction and is almost invariable with TOS, which is substantially different from the trend found in the latter zeolite. Furthermore, H-FER-L produces a higher amount of propene and pentenes than H-FER-S and shows no significant changes in selectivity to these two major by-products with increasing TOS. These results strongly suggest that with prolonged TOS, the catalytic action of H-FER-L is still dominated by the acid sites located inside the zeolite pores, where nonselective dimerization-cracking reactions must be predominant, and that there are no changes in the prevailing mechanism over the period of time studied here. To further clarify the point given above, we have performed additional catalytic experiments on the H-FER-L zeolite treated with oxalic acid for 24 h and found essentially the same catalytic behavior as that obtained from the parent H-FER-L during 8 h on stream, confirming that the prevailing mechanism over aged H-FER-L is different from that over aged H-FER-S. It is thus clear that the 1-butene selectivity of aged H-FER could be at least qualitatively correlated with the density of the Brønsted acid sites located near the 10-ring pore mouths. On the other hand, no detectable differences in the 1-butene conversion, as well as in the selectivity to isobutene or to by-products, over the period of TOS studied are observed, when H-ZSM-5-L is compared with H-ZSM-5-S under the same reaction conditions. This again shows that the ZSM-5 10-ring pores are large enough to efficiently accommodate *n*-butene molecules, even if high amounts of coke were already deposited.

A next logical step would be to discuss the role of coke deposits in the 1-butene skeletal isomerization over H-FER which is typically prepared with a small crystal size, like our H-FER-S zeolite. Here we start our discussion on this topic based on the two following points of view that are simple but have been relatively neglected in the literature: (1) H-FER should be effectively a one-dimensional 10-ring material as far as the 1-butene skeletal isomerization is concerned, because of the small pore diameter (3.5×4.8 Å) of its 8-ring channels where the diffusion coefficients of butene isomers are not significant compared to those associated with 10-ring (4.2×5.4 Å) channels; and (2) even soft coke molecules, once they are formed over one acid site inside the 10-ring channels in H-FER, may grow with dimensions that are sufficient to inhibit the diffusion of 1-butene (3.0×4.7 Å) or isobutene (3.3×4.1 Å) molecules to the remaining acid sites lined along the same channel, rendering them inaccessible for catalysis. If these two points are sensible hypotheses, then pore blockage by coke deposits

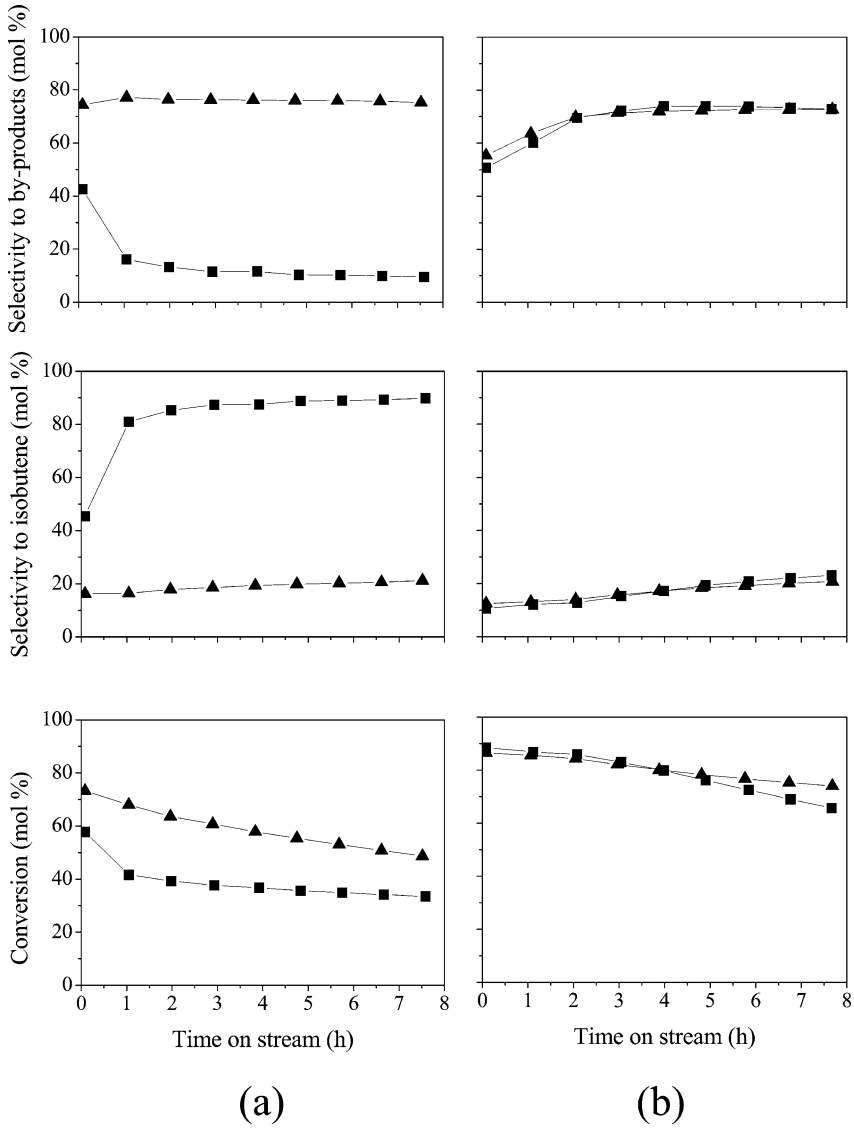

Fig. 5. 1-Butene conversion (bottom) and selectivities to isobutene (middle) and propene plus pentenes (top) as a function of time on stream in skeletal isomerization of 1-butene over (a) H-FER and (b) H-ZSM-5 with small (squares) and large (triangles) crystal sizes. The reaction conditions are the same as those given in Fig. 1.

should significantly decrease the probability of coverage deactivation of the individual acid sites located inside the FER pores. This implies that the pore-blocking role [5,10,48,49] of coke deposits may be more important than their role in selectively poisoning the very strong acid sites inside the FER pores [10,49]. Due to the reasons described above, on the other hand, creation of new highly selective isomerization sites on the coke molecules located near the FER pore mouths [11–13] cannot be the definite explanation for the observed increase in isobutene selectivity. This appears to be also the case of alterations in FER pore dimensions by coke deposits [9,10,49], especially taking into account the catalytic results from a high-silica H-FER (Si/Al = 59) by Asensi and Martinez [46]. Finally, coking of the nonselective acid sites on the external surface of H-FER crystals [5,50] could lead to some enhancement of isobutene selectivity. However, this cannot be the major contributing factor because the number of acid sites on the external surface of typical zeolite crystals is much smaller than that of acid sites in their intracrystalline space. In any case, if the rapid increase of isobutene selectivity over H-FER with increasing TOS is a consequence of suppression of nonselective dimerization-cracking reactions, this intriguing phenomenon could be understood mainly in terms of a decrease in the density of the Brønsted acid sites located inside the FER pores with coke deposition, over which the bimolecular mechanism is preferentially operating, and more likely in their accessibility due to pore blockage.

Recently, van Donk et al. [17,36,40,41] have monitored the buildup of coke in H-FER during the course of 1-butene skeletal isomerization using several analytical tools, such as TEM, electron energy loss spectroscopy (EELS), and in situ IR spectroscopy, and found that the 10-ring pore mouth inlets are still accessible for 1-butene molecules even under

the conditions in which a considerable amount of coke has already built up on the outer surface of H-FER crystals, as well as near the 8-ring pore mouths. This indicates that the rate of coke formation on H-FER differs significantly according to the intrazeolitic location of acid sites. If such is the case, it should then be noted here that the amount (5.6%) of coke deposited on H-FER-L is considerably smaller than that (8.9%) on H-FER-S, while no significant differences in the amount ($\sim$ 6%) of coke formed are observed for H-ZSM-5-L and H-ZSM-5-S (Table 1). Recall that these two pairs of zeolites with small and large crystal sizes have similar bulk Si/Al ratios, respectively. It is thus appears that the rate of coke formation on zeolites can also depend on the crystal size of these microporous materials, as well as on their pore architecture and acidity [44,45], although there is currently little understanding of the correlation between coke formation and zeolite crystal size. Considering that the general catalytic behavior of H-CLI is similar to that of H-FER, on the other hand, one cannot claim that pore mouth catalysis is unique with H-FER among the already known 10-ring zeolites. Based on the overall catalytic results of our study, however, we believe that the 10-ring pores of H-FER may have a more suitable degree of ellipticity of 10-ring channels in more effectively chemisorbing *n*-butene molecules near the pore mouths than the other 10-ring zeolites studied here.

4. Conclusions

The catalytic activities of the proton form of a series of 10-ring zeolites including clinoptilolite, ferrierite, ZSM-22, SUZ-4, ZSM-57, and ZSM-5 for the skeletal isomerization of 1-butene to isobutene, as well as those of the dealuminated analogs of some of these zeolites that were prepared via oxalic acid treatment, are presented. Analysis of the catalytic data obtained from these zeolites suggests that the remarkable isobutene selectivity of aged H-ferrierite can be explained by pore mouth catalysis which takes over the Brønsted acid sites near its 10-ring pore mouth inlets with a suitable degree of ellipticity. Further evidence to support this speculation has been drawn by comparing the isomerization activities of two H-ferrierite zeolites having the similar Si/Al ratios but notably different crystal sizes and thus different numbers of 10-ring pore mouths per unit weight. It appears that the main role of coke deposits formed during the reaction over H-ferrierite lies in the blockage of 10-ring channels except their both ends, which makes most of the intrazeolitic voids unavailable for nonselective dimerization-cracking reactions. We believe that this may result from the behavior of this particular zeolite that is normally synthesized with a submicrometer crystal size, as well as from its unique pore structure.

Acknowledgment

Funding for this work was provided by the Korea Science and Engineering Foundation under Grant R02-2003-000-10087-0 to S.B.H.

References

[1] V.R. Choudary, Chem. Ind. Dev. 8 (1974) 32.
[2] A.C. Butler, C.P. Nicolaides, Catal. Today 18 (1993) 443.
[3] P. Grandvallet, K.P. de Jong, H.H. Mooiweer, A.G.T.G. Kortbeek, B. Kraushaar-Czarnetzki, W.H.J. Stork, B.C.H. Krutzen, Eur. patent 501,577, 1992.
[4] H.H. Mooiweer, K.P. de Jong, B. Kraushaar-Czarnetzki, W.H.J. Stork, B.C.H. Krutzen, Stud. Surf. Sci. Catal. 84 (1994) 2327.
[5] W.-Q. Xu, Y.-G. Yin, S.L. Suib, J.C. Edwards, C.-L. O'Young, J. Phys. Chem. 99 (1995) 9443.
[6] R.J. Pellet, D.G. Casey, H.-M. Huang, R.V. Kessler, E.J. Kuhlamn, C.-L. O'Young, R.A. Sawicki, R.J. Ugolini, J. Catal. 157 (1995) 423.
[7] P. Meriaudeau, R. Bacaud, L.N. Hung, V.A. Tuan, J. Mol. Catal. 110 (1996) L177.
[8] K.P. de Jong, H.H. Mooiweer, J.G. Buglass, P.K. Maarsen, Stud. Surf. Sci. Catal. 111 (1997) 127.
[9] G. Seo, H.S. Jeong, D.-L. Jang, D.L. Cho, S.B. Hong, Catal. Lett. 41 (1996) 189.
[10] J. Houzvicka, V. Ponec, Ind. Eng. Chem. Res. 36 (1997) 1424.
[11] M. Guisnet, P. Andy, N.S. Gnep, E. Benazzi, C. Travers, J. Chem. Soc., Chem. Commun. (1995) 1685.
[12] M. Guisnet, P. Andy, N.S. Gnep, E. Benazzi, C. Travers, J. Catal. 158 (1996) 551.
[13] P. Andy, N.S. Gnep, M. Guisnet, E. Benazzi, C. Travers, J. Catal. 173 (1998) 322.
[14] G. Seo, M.-Y. Kim, J.-H. Kim, Catal. Lett. 67 (2000) 207.
[15] J. Houzvicka, V. Ponec, Catal. Rev. Sci. Eng. 39 (1997) 319.
[16] P. Meriaudeau, C. Naccache, Adv. Catal. 44 (1999) 505.
[17] S. van Donk, J.H. Bitter, K.P. de Jong, Appl. Catal. A 212 (2001) 97.
[18] S.L. Lawton, J.M. Bennett, J.L. Schlenker, M.K. Rubin, J. Chem. Soc., Chem. Commun. (1993) 894.
[19] M.A. Asensi, M.A. Camblor, A. Martinez, Micropor. Mesopor. Mater. 28 (1999) 427.
[20] M.R. Apelian, A.S. Fung, US patent 5,242,676, 1993.
[21] M.R. Apelian, A.S. Fung, G.J. Kenndy, T.F. Degnan, J. Phys. Chem. 100 (1996) 16577.
[22] G. Seo, M.-W. Kim, J.-H. Kim, B.J. Ahn, S.B. Hong, Y.S. Uh, Catal. Lett. 55 (1998) 105.
[23] C.J. Plank, E.J. Rosinski, M.K. Rubin, US patent 4,016,245, 1977.
[24] P.A. Jacobs, J.A. Martens, Stud. Surf. Sci. Catal. 33 (1987) 24.
[25] W.C. Paik, C.-H. Shin, S.B. Hong, Chem. Commun. (2000) 1609.
[26] S.-H. Lee, D.-K. Lee, C.-H. Shin, W.C. Paik, W.M. Lee, S.B. Hong, J. Catal. 196 (2000) 158.
[27] T.J. Kim, W.S. Ahn, S.B. Hong, Micropor. Mater. 7 (1996) 35.
[28] J.L. Guth, H. Kessler, R. Wey, Stud. Surf. Sci. Catal. 28 (1986) 121.
[29] F.C. Meunier, L. Domokos, K. Seshan, J.A. Lercher, J. Catal. 211 (2002) 366.
[30] P. Meriaudeau, A. Vu Tuan, N. Le Hung, G. Szabo, Catal. Lett. 47 (1997) 71.
[31] S.-H. Lee, D.-K. Lee, C.-H. Shin, Y.K. Park, P.A. Wright, W.M. Lee, S.B. Hong, J. Catal. 215 (2003) 151.
[32] W.H. Beyer, CRC Standard Mathematical Tables, twenty eighth ed., CRC, Boca Raton, FL, 1987.
[33] R. Byggningsbacka, N. Kumar, L.-E. Lindfors, J. Catal. 178 (1998) 611.
[34] P. Meriaudeau, A. Vu Tuan, N. Le Hung, C. Naccache, G. Szabo, J. Catal. 171 (1997) 329.
[35] B.S. Kwak, J. Sung, Catal. Lett. 53 (1998) 125.

[36] S. van Donk, E. Bus, A. Broersma, J.H. Bitter, K.P. de Jong, Stud. Surf. Sci. Catal. 142 (2002) 573.
[37] J.A. Martens, R. Parton, L. Uytterhoven, P.A. Jacobs, Appl. Catal. 76 (1991) 95.
[38] S.J. Miller, Micropor. Mater. 2 (1994) 439.
[39] J.A. Martens, W. Souverijins, W. Verrelst, R. Parton, G.F. Froment, P.A. Jacobs, Angew. Chem. Int. Ed. 34 (1995) 2528.
[40] S. van Donk, E. Bus, A. Broersma, J.H. Bitter, K.P. de Jong, J. Catal. 212 (2002) 86.
[41] S. van Donk, E. Bus, A. Broersma, J.H. Bitter, K.P. de Jong, Appl. Catal. A 237 (2002) 149.
[42] C.-L. O'Young, R.J. Pellet, D.G. Casey, R.J. Ugolini, R.A. Sawicki, J. Catal. 151 (1995) 467.
[43] D. Brouwer, J. Oelderik, Rec. Trav. Chim. Pays-Bas 87 (1968) 1435.
[44] N.Y. Chen, T.F. Degnan Jr., C.M. Smith, Molecular Transport and Reaction in Zeolites, VCH, New York, 1994.
[45] H.G. Karge, Stud. Surf. Sci. Catal. 137 (2001) 707.
[46] M.A. Asensi, A. Martinez, Appl. Catal. A 183 (1999) 155.
[47] L. Domokos, L. Lefferts, K. Seshan, J.A. Lercher, J. Catal. 197 (2001) 68.
[48] J.W. Beeckman, G.F. Froment, Ind. Eng. Chem. Fundam. 1 (1991) 245.
[49] W.-Q. Xu, Y.-G. Yin, S.L. Suib, C.-L. O'Young, J. Phys. Chem. 99 (1995) 758.
[50] P. Meriaudeau, C. Naccache, L.N. Hung, V.A. Tuan, G. Szabo, J. Mol. Catal. A 123 (1997) L1.